

1     **Seasonal and Radial Trends in Saturn’s Thermal Plasma Between the Main Rings**  
2    **and Enceladus**

3  
4                    M.K. Elrod<sup>1,2</sup>, W-L Tseng<sup>3</sup>, A. K. Woodson<sup>1</sup>, R. E. Johnson<sup>1</sup>

5  
6                                    <sup>1</sup> University of Virginia, Charlottesville, VA  
7                                    <sup>2</sup> National Institute of Aerospace, Hampton, VA  
8                                    <sup>3</sup> Southwest Research Institute, San Antonio, TX

9  
10  
11  
12  
13  
14    **Abstract**

15            A goal of Cassini’s extended mission has been to examine the seasonal variations  
16 of Saturn’s magnetosphere, moons, and rings. Recently we showed that the  
17 magnetospheric plasma between the main rings and Enceladus exhibited a time  
18 dependence that we attributed to a seasonally variable source of oxygen from the main  
19 rings (*Elrod et al.*, 2012). Such a temporal variation was subsequently seen in the  
20 energetic ion composition (*Christon et al.*, 2013). Here we include the most recent  
21 measurements by the Cassini Plasma Spectrometer (CAPS) in our analysis (*Elrod et al.*,  
22 2012) and modeling (*Tseng et al.*, 2013a) of the temporal and radial dependence of the  
23 thermal plasma in the region between the main rings and the orbit of Enceladus. Data  
24 taken in 2012, well past equinox for which the northern side of the main rings were  
25 illuminated, appear consistent with a seasonal variation. Although the thermal plasma in  
26 this region comes from two sources, the extended ring atmosphere and the Enceladus  
27 torus that have very different radial and temporal trends, the heavy ion density is found to  
28 exhibit a steep radial dependence that is similar for all years examined. Using our  
29 chemical model, we show that this dependence requires a radial dependence for  
30 Enceladus torus that differs from recent models or, more likely, enhanced heavy ion  
31 quenching with decreasing distance from the edge of the main rings. We examine the  
32 possible physical processes and suggest that the precipitation of the inward diffusing  
33 high-energy background radiation onto the edge of the main rings could play an  
34 important role.

## 35 1. Introduction

36 The thermal plasma in the inner magnetosphere, from just outside the main rings  
37 to just inside the orbit of Enceladus ( $\sim 2.4R_S - 3.8R_S$ ;  $1 R_S = 1$  Saturn Radius =  
38 60,300km), is studied using Cassini Plasma Spectrometer (CAPS) data from 2004  
39 through 2012. The goal of this paper is to further examine the temporal and radial  
40 variation in the heavy ion plasma (*Elrod et al.*, 2012). The  $O_2^+$  observed by the CAPS  
41 instrument over the main rings (*Tokar et al.*, 2006) was suggested to be formed from  $O_2$   
42 produced by photo-decomposition of the icy ring particles (*Johnson et al.*, 2006a). A  
43 fraction of this  $O_2$  is subsequently scattered, forming an extended ring atmosphere, in  
44 which the molecules are ionized contributing to the plasma in Saturn's inner  
45 magnetosphere (e.g., *Johnson et al.*, 2006a; *Martens et al.*, 2008). Since such a source  
46 depends on the illumination of the ring plane, the plasma density was predicted to vary  
47 over Saturn's orbit as the ring plane illumination varied from the southern hemisphere  
48 through equinox to the northern hemisphere (*Tseng et al.*, 2010; 2013a). Water group  
49 ions, labeled here as  $W^+$  ( $O^+$ ,  $OH^+$ ,  $H_2O^+$ , and  $H_3O^+$ ) are also directly formed in this  
50 region by ionization of neutrals in the Enceladus torus (*Cassidy et al.*, 2010; *Smith et al.*  
51 2010; *Tseng et al.*, 2012). While this source probably does not exhibit a seasonal  
52 variation, there is evidence that it fluctuates by up to a factor of four (*Smith et al.*, 2010)  
53 and appears to depend on the position of Enceladus in its orbit (*Hedman et al.* 2013).

54 In *Elrod et al.* (2012) we used CAPS data from SOI to 2010 to confirm that the  
55 main rings are an important source of  $O_2^+$  and  $O^+$  ions inside the orbit of Mimas. We also  
56 showed that there was a steep drop in  $O_2^+$  density, as well as in the total heavy ion  
57 thermal plasma, over that time period. Consistent with this, the Magnetospheric

58 Imaging Instrument (MIMI) recently reported a decrease from SOI through 2010 in  
59 energetic  $O_2^+$  density as compared to the  $W^+$  density, followed by a recovery in 2011-  
60 2012 (*Christon et al.*, 2013). More recently a seasonal variation was reported equatorial  
61 electron densities measured by the Radio and Plasma Wave Instrument (RPWS) (Persoon  
62 et al. 2013a).

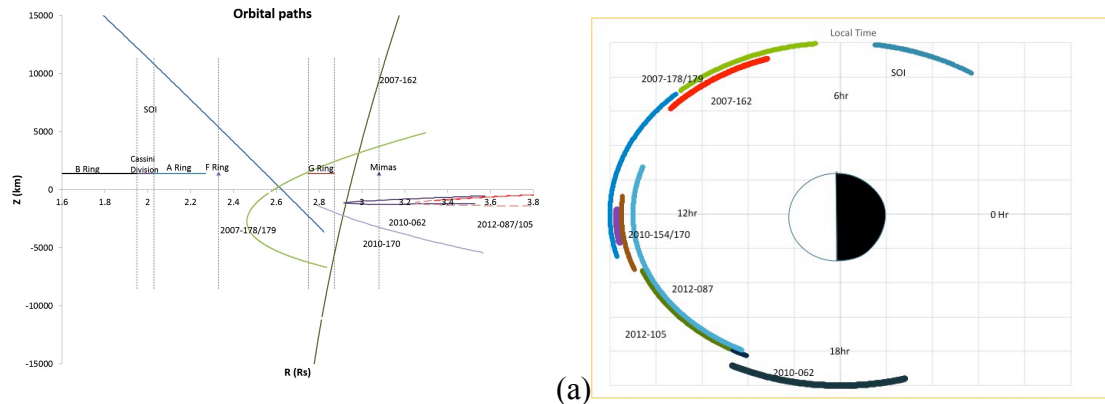
63 The present study of the thermal plasma extends our earlier time frame by  
64 including the 2012 data in order to determine whether or not the density increases after  
65 equinox. Because seasonal variations were assumed to be due to a ring atmosphere source  
66 superimposed on the Enceladus torus source, the seasonal variation might be expected to  
67 decrease with distance from the main rings consistent with models of the ring  
68 atmosphere. Surprising for all the years studied, the total *heavy ion* density, as well as  
69 that for the individual  $O_2^+$  and  $W^+$  ions, increases relatively steeply with increasing  
70 distance from Saturn. This is the case even though the proposed seasonal variation is  
71 thought to be primarily due to molecules scattered from the ring atmosphere. After  
72 presenting the new results, we consider the implications of these findings.

73

## 74 **2. Analysis**

75 In order to study the temporal and radial variation in the density and composition  
76 of the thermal plasma, we examined passes from SOI in 2004, two in 2007 (doy 162 &  
77 178/179), three in 2010 (doy 062, 154, and 170), and two in 2012 (doy 087 and 105) in  
78 the region between  $\sim 2.4 R_S - 3.8 R_S$  ( $1 R_S = 1$  Saturn Radius = 60,300km). All of these  
79 passes had a periapsis within the Enceladus orbit at  $\sim 4.0 R_S$  and had near equatorial  
80 segments which we focus on here. In Fig.1 we show both the orbital paths in the  $R$  vs.  $Z$

81 plane and the local time for each of the passes used in this study. Although there is a  
 82 significant spread in local time, with the exception of SOI, all the passes were on the  
 83 dayside, reducing the importance of the suggested night to day variations seen by the  
 84 Cassini Radio and Plasma Wave Science (RPWS) Langmuir probe (*Holmberg et al.*,  
 85 2013).



86

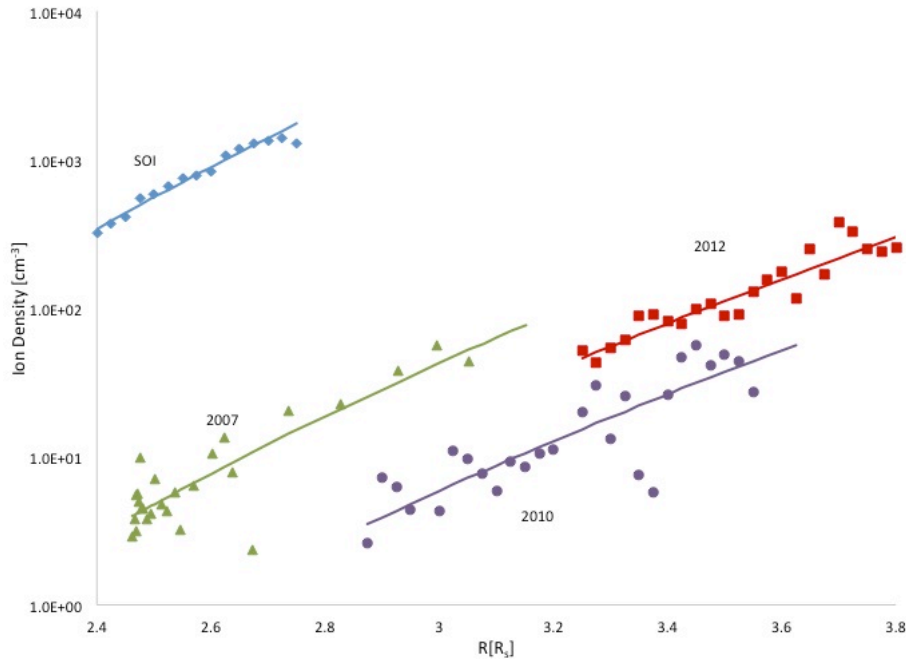
(a)

87 (b)

88 Figure 1. Orbits used in this study: a) Position in equatorial radius,  $R$  in  $R_s$  ( $1R_s \approx 60,300$  km in the  
 89 equatorial plane) vs. distance above the equator,  $Z$  in km; for consistency in the comparisons and to  
 90 maximize the count rate, the data presented below comes from the near equatorial segments ( $Z$  within  
 91  $\pm 5,000$  km). b) Local times during each orbit. With the exception of SOI, most of the data was taken on the  
 92 dayside between dawn and dusk.  
 93

94 In *Elrod et al. (2012)* we described the method of analyzing the CAPS singles  
 95 data, the correction for the significant background in this region, and the fitting of the  
 96 measured energy spectrum to obtain the total ion densities as well as the  $O_2^+$  and  $W^+$   
 97 fractions. These details are not repeated here. Unlike in *Elrod et al. (2012)* we only  
 98 analyzed CAPS singles data taken close to the equator, having a minimum number of A-  
 99 cycles, and at least 400 counts above background in order to reduce the scatter in the  
 100 data. We also included the 2012 data, which was not available earlier. Although there are  
 101 variations in the total heavy ion density observed between those passes in Fig. 1

102 occurring in the same year, which we will examine in the future, these variation are  
 103 typically smaller than the variations between years. Therefore, we show in Fig. 2 the  
 104 average of the total heavy ion density for each year vs. radial distance from Saturn for  
 105 those segments close to the equator ( $Z < 5000\text{km}$ ).  
 106

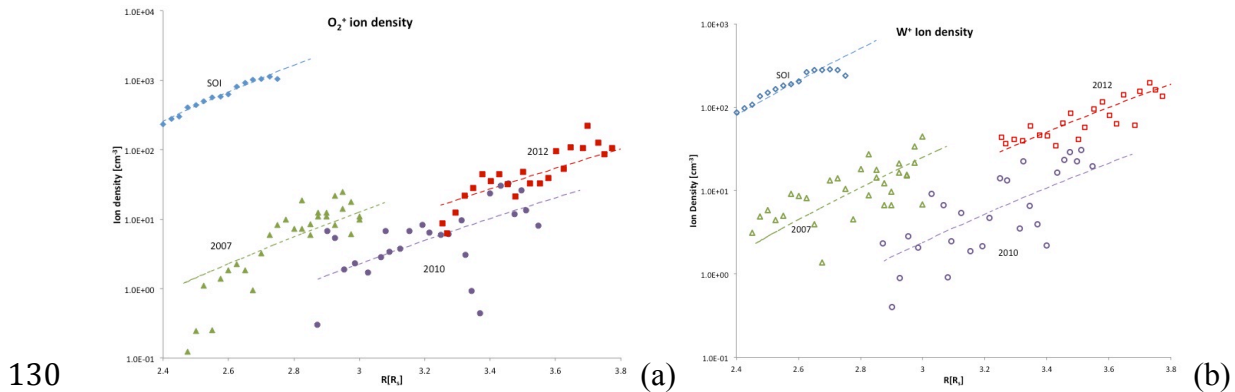


107  
 108 Figure 2. Total heavy ion densities vs.  $R$  in  $R_s$  from 2004 through 2012 averaged over orbits for each year  
 109 in Fig. 1a: SOI in 2004 (blue diamonds), 2007 (green triangles), 2010 (purple dots), and 2012 (red squares).  
 110 Lines are fits:  $n_i = c(R/3R_s)^{1/2}$ ; where  $c$  is the extrapolated value  $n_i(3R_s)$ : (SOI) blue [ $c=4.94 \times 10^3 / \text{cm}^3$ ], 2007  
 111 green [ $c=42.5 / \text{cm}^3$ ], 2010 purple [ $c=5.85 / \text{cm}^3$ ], and 2012 orange [ $c=17.5 / \text{cm}^3$ ].  
 112

113 It is seen in Fig. 2 that there is a clear decrease in the heavy ion density from 2004  
 114 through 2010 and an increase from 2010 to 2012. Therefore, the lowest densities occur in  
 115 2010, the orbit closest to equinox (11 August, 2009) with apparent recovery through  
 116 2012. It is also seen that all densities, regardless of year, increase radially outward. While  
 117 there are significant changes in the magnitude of the densities between the years, the  
 118 radial dependence of each of these sets is remarkably similar. In order to better quantify  
 119 the data we fit a power law in equatorial distance from Saturn,  $R$ , to each of these

120 averaged data sets. The steep variation is roughly fit using the form  $n_i = c (R/3R_S)^{12}$ .  
 121 Because the radial range is narrow, powers varying from ~10-14 also give reasonable  
 122 descriptions. We use a power of 12 in the following and note that the measured radial  
 123 dependence is relatively steep.

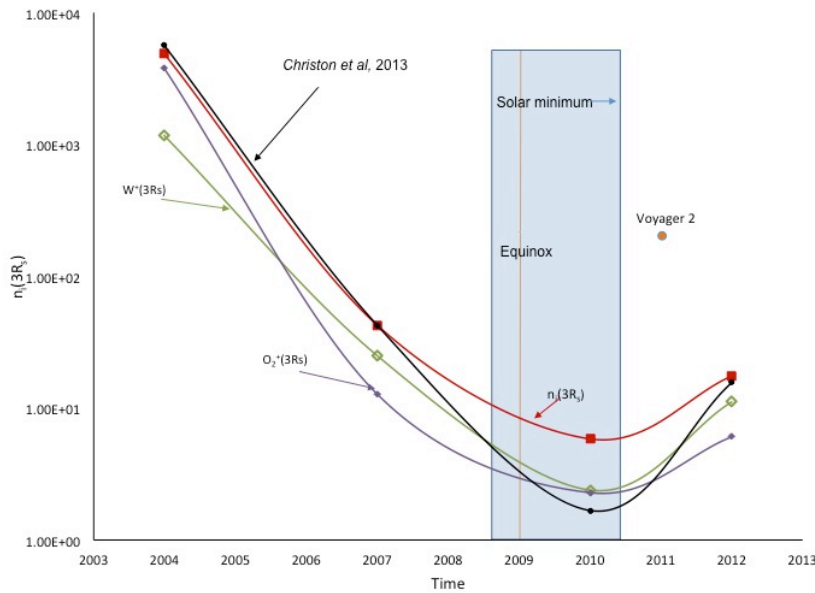
124 As discussed below, the SOI data is dominated by  $O_2^+$ , likely from the extended  
 125 ring atmosphere, with temperatures close to the fresh ion pick-up temperature, whereas  
 126 the later data sets, closer to equinox, are dominated by  $W^+$ , likely from the Enceladus  
 127 torus, but with low ion temperatures (*Elrod et al.*, 2012). In spite of the different  
 128 compositions and temperatures, there is a striking similarity in the radial dependence in  
 129 all of the years studied.



131 Figure 3. Averaged densities for each year: (a)  $O_2^+$ , closed symbols; (b)  $W^+$  ( $O^+, OH^+, H_2O^+, H_3O^+$ ), open  
 132 symbols: SOI in 2004 (blue diamonds), 2007 (green triangles), 2010 (purple dots), 2012 (red squares). As in  
 133 Fig. 2 the lines are fits:  $n_i(R) = c (R/3R_S)^{12}$ . The extrapolated values  $c \approx n_i(3R_S)$  in  $cm^{-3}$  for  $O_2^+$  and  $W^+$   
 134 respectively: (2004:  $3.8 \times 10^3$ ,  $1.2 \times 10^3$ ), (2007: 12.8, 25.0), (2010: 2.3, 2.4) and (2012: 6.06, 11.2).  
 135

136 Using the analysis in *Elrod et al.* (2012) with the selectivity discussed here, we  
 137 also show the yearly averaged  $O_2^+$  and  $W^+$  components of the density in Figs. 3a and b.  
 138 Because the peaks in the CAPS singles spectra overlap significantly, these data have a  
 139 much larger scatter, but still exhibit a radial dependence roughly similar to that in Fig. 2.  
 140 Therefore, we also fit each set using  $n_i = c (R/3R_S)^{12}$ . It is seen to capture the general

141 trend with the exception of the  $O_2^+$  2007 data at the smallest values of  $R$ . None of these  
 142 fits are unique, as the  $O_2^+$  data can be better fit on average with a slightly smaller power  
 143 and the  $W^+$  with a slightly larger power. Here we use the rough fits in Figs. 2 and 3 to  
 144 guide the discussion below.



145

146 Figure 4. Extrapolated densities at  $3R_S$ ,  $n_i(3R_S)$  vs. year, obtained from the value of  $c$  from the fits in Figs. 2  
 147 and 3: (red) total heavy ion density from Fig. 2; (purple)  $O_2^+$  and (green)  $W^+$  from Fig. 3. Lines are drawn to  
 148 guide the eye. Using powers of 9.8 and 14.1, which gave slightly better fits to the  $O_2^+$  and  $W^+$  respectively  
 149 changed these values by  $\sim 10\%$ . (Black line)  $O_2^+/W^+$  ratio from MIMI data (Christon et al., 2013) times  
 150 our  $W^+$  data. Red dot: Voyager 2 total ion density Aug. 1981, one year after equinox but close to solar  
 151 maximum. Orange vertical line marks equinox in August of 2009. The grey rectangle marks the region of  
 152 solar minimum: late 2008 through mid-2010.

153

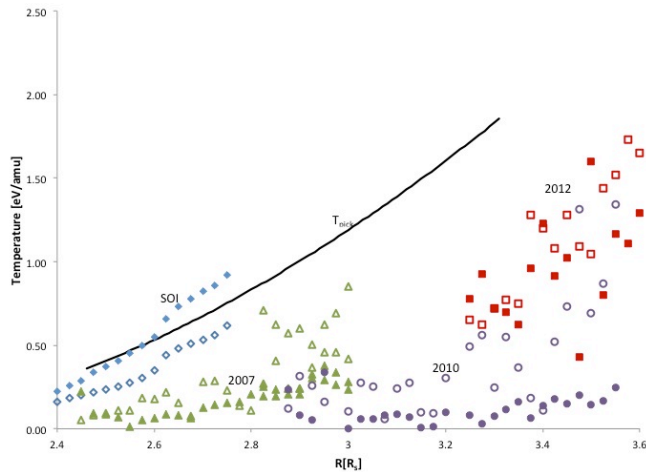
154 In Fig. 4 we plot the fit coefficients,  $c$ , from Figs. 2 & 3. These are essentially the  
 155 extrapolated values of the averaged density for each year in the middle of the radial range  
 156 considered here,  $n_i(3R_S)$ . Since the ionization rate throughout much of our region is  
 157 dominated by photo-ionization (e.g., Sittler et al., 2008) we also indicate the rough extent  
 158 of solar minimum by the grey band and equinox by the vertical line. It is seen that these  
 159 densities all drop from closest to solstice in 2004 through 2010, closest to equinox and  
 160 roughly within the solar minimum, and then increase again in 2012. It is also seen that

161  $O_2^+$  dominates at SOI, whereas  $W^+$  dominates in the later years (*Elrod et al.*, 2012)  
162 allowing for the significant scatter in the data. A fraction of the  $O_2^+$  and  $W^+$  produced  
163 throughout the magnetosphere gets accelerated to high energies. Therefore, *Christon et*  
164 *al.* (2013) also saw a clear seasonal dependence in the  $O_2^+/W^+$  ratio in the MIMI data.  
165 Rather than compare their ratio to our densities, we multiply our  $W^+$  data by the ratio and  
166 display it in Fig. 4. It is seen that the trends are very similar and the post-equinox increase  
167 appears to be delayed in both sets of data. This delay is at least in part due to the fact that  
168 the northern illumination was predicted to produce a less robust extended ring  
169 atmosphere than southern illumination at the same solar inclination angle (*Tseng et al.*,  
170 2010).

171         Since the recent period of solar minimum occurred close to equinox, the EUV/UV  
172 ionization rate also goes through a minimum in the time period indicated in Fig. 4. The  
173 photo-ionization rate of  $H_2O$  can therefore change by a factor of the order of few (e.g.,  
174 *Huebner et al.*, 1992). Since solar maximum occurred in about 2000, clearly some of the  
175 variation seen in Fig. 4 is due to the changing ionization rate from near the middle of the  
176 solar cycle at SOI to a minimum from late 2008 through mid 2010 and then increasing in  
177 2011. Because the EUV/UV photons also determine the photon-induced decomposition  
178 of the icy ring particles, the extended the ring atmosphere varies in this time period  
179 somewhat faster than predicted in *Tseng et al.* (2010). However, the drop in the thermal  
180 plasma density in Fig. 4 is much too large to be accounted for by the change in the solar  
181 flux alone. To help separate the seasonal and solar cycle effects, we include the equatorial  
182 Voyager 2 plasma density taken about a year after equinox in August 1981, but close to  
183 *solar maximum* (*Elrod et al.*, 2012). Although the state of the magnetosphere differed,



184 affecting the electron impact contribution to ionization, and the instrument sensitivities  
 185 differ, the comparison suggests that the solar ionizing flux is important, but is not the  
 186 dominant cause of the temporal variations in the thermal plasma seen in Fig. 4.



187

188 Figure 5. Extracted ion temperatures in (eV/amu) vs.  $R$  in  $R_S$ : for  $O_2^+$  and  $W^+$  as indicated. Solid line: pick-  
 189 up temperature/amu for ions freshly formed from a neutral in a circular orbit. The significant scatter in the  
 190 data is roughly consistent with the uncertainties, not shown for clarity.

191

192 In Fig. 5 we show the ion temperatures,  $T_i$ , for the two species determined from  
 193 the peak widths. Because the  $O_2^+$  and  $W^+$  peaks in the CAPS singles data have  
 194 considerable overlap (*Elrod et al., 2012; Elrod 2013*) there is a significant amount of  
 195 scatter in these results. However, the trend is clear. At SOI the  $O_2^+$  temperatures are close  
 196 to the pick-up temperature calculated for ions freshly formed from neutrals in roughly  
 197 circular, Keplerian orbits. This indicates the lifetimes are short compared to collisional  
 198 cooling, reaction and recombination processes. This is not the case for the other years for  
 199 which the temperatures for each species are a fraction of the pick-up temperature, a trend  
 200 that continued in our most recent 2012 data. As proposed in *Tseng et al. (2013a)*, this is  
 201 due to the rapid ion-neutral interactions in this region where the relative ion-neutral  
 202 speeds are relatively low.

203

204 **3. Discussion of the Results**

205 Earlier we developed a one-box homogeneous ion chemistry model to account for  
206 the complex and highly variable plasma environment (i.e. density, composition, and  
207 temperature) observed near equator between the main rings and Enceladus (*Tseng et al.*,  
208 2013a). We used models of the Enceladus torus as a source for the water group ions, the  
209 scattered ring atmosphere and the Enceladus torus as sources of the light ions,  $H^+$  and  
210  $H_2^+$ , and the scattered ring atmosphere as a source for  $O^+$  and  $O_2^+$ . The density of the  
211 Enceladus torus, although varying in its orbit, does not appear to have a seasonal  
212 variability (*Smith et al.*, 2010), but the extended ring atmosphere was predicted to vary  
213 due to the changing orientation of the ring plane to the flux of solar UV photons as Saturn  
214 orbits the sun (*Tseng et al.*, 2010). Here we again use this model and refer the reader to  
215 *Tseng et al.* (2013a) for the list of reactions and other details.

216 Solving a set of chemical rate equations, we showed that the observed temporal  
217 variations in the near equatorial *average* in the total heavy ion density and  $O_2^+$  density  
218 were primarily seasonal due to the predicted variation in the ring atmosphere. The model  
219 also *required* an enhancement at SOI caused by a compressed magnetosphere producing  
220 an enhanced hot electron component. Due to the low relative ion speeds in this region,  
221 the ion–neutral collisions determined both the composition and the surprisingly low ion  
222 temperatures found after SOI as seen in Fig. 5. Even though  $O_2$  from the extended ring  
223 atmosphere is the dominant source of  $O_2^+$  at SOI, we also showed that  $O_2^+$  is formed by  
224 ion-molecule reactions in the magnetosphere, so is present at some level even where the  
225 contribution from the extended ring atmosphere is small. Using the dust densities in this

226 region detected by the Cassini Cosmic Dust Analyzer (CDA)(*Kempf et al.*, 2008), the  
227 effect of the ion–dust interactions was found to be unimportant.

228 Our chemical model was applied at an average radial distance,  $\sim 3R_S$ , and, as  
229 stated above, appears to account for the *averaged* plasma densities, composition and  
230 temperatures as a function of the season. However, the radial dependence of the ion  
231 densities was not examined. Here we show that in going from southern solstice through  
232 equinox and onto illumination of the northern side of the ring plane (2004-2012) the  
233 radial dependence of these yearly averaged total ion density increases with increasing  
234 distance from Saturn as seen in Figs. 2 and 3. Surprisingly, this was found to be the case  
235 whether the plasma was dominated by  $O_2^+$ , as at SOI, or by  $W^+$ . This dependence is much  
236 steeper than the radial dependence of the neutral density in the Enceladus torus (*Cassidy*  
237 *and Johnson*, 2010) and is *opposite* to the radial dependence of the extended ring  
238 atmosphere (*Tseng et al.*, 2010). Using even a simple model of reaction pathways, which  
239 includes a diffusion time, and the neutral sources, the resulting ion density at equinox  
240 varies only slowly with  $R$  when using the Enceladus torus source in *Cassidy and Johnson*  
241 (2010). Since the average ion densities were about right, either the radial dependence of  
242 neutral sources are significantly in error or a quenching mechanism that becomes more  
243 important with decreasing distance from the main rings is absent or incorrect.

244 The difference in the spatial morphology of the source rate and the heavy ion  
245 density is especially evident in the SOI data when the plasma is heavily dominated by  
246  $O_2^+$  with temperatures close to the pick-up energy. The latter indicates, as stated above,  
247 that these ions, formed from oxygen in the extended ring atmosphere, have short  
248 lifetimes. The neutral oxygen source clearly decreases with distance from the main rings.

249 However, it is seen in Fig. 3a that the  $O_2^+$  density increases with increasing  $R$  over the  
250 narrow range of  $R$  for which there is data. Below we consider those processes that might  
251 produce the observed radial dependences from 2004 to 2012.

#### 252 **4. Radial Dependence**

253 We focus here on the radial variation in the near equatorial densities in Fig. 2.  
254 Although the heavy ion data in 2010, nearest to equinox varies between  $\sim 4$  to  $\sim 40/\text{cm}^3$  in  
255 going from  $\sim 2.9$  to  $\sim 3.5R_s$ , the ion-chemistry model in *Tseng et al. (2013a)* gives heavy  
256 ion densities that are nearly independent of  $R$  ( $\sim 25/\text{cm}^3$  with a slight minimum at  $2.75R_s$ ).  
257 Below we discuss the possible reasons for the difference between the model and  
258 measured radial dependence. Before proceeding, we note that heavy ion density in a flux  
259 tube (density vertically integrated along a field line) at each  $R$  is more closely related to  
260 the ionization source rate than is the equatorial density. It can be roughly estimated as the  
261 equatorial density times the scale height which is proportional to  $\sim T_i^{1/2}$ . Because the ion  
262 temperature in Fig. 5 increases with increasing  $R$ , the flux tube content would exhibit an  
263 even steeper radial dependence than the near equatorial densities in Fig. 2. Therefore, the  
264 difference in the morphology of the heavy ion flux tube content and the spatial  
265 morphology of the sources would be even more dramatic.

266 In *Tseng et al. (2013a)* the averaged ion-molecule collisions and ion-electron  
267 recombination processes had timescales near equinox of a  $\sim 10^5$ s throughout this region  
268 and  $\sim 10^4$ s at SOI inside of  $\sim 2.8R_s$ . Therefore, processes that might account for the steep  
269 decay with decreasing  $R$  must have shorter time scales. For example, using the fit to the  
270 2010 data in Fig. 2, a quenching process that accounts for the observed radial dependence  
271 can have a longer time scale, greater than a few times  $10^5$ s at  $\sim 3.5R_s$ . However, at  $\sim 2.5R_s$

272 our data would require a time scale  $\sim 5 \times 10^4$ s. That is, to account for the steep radial  
273 dependence, the lifetime of the heavy ions produced must be smallest closest to the edge  
274 of the rings. Although we do not determine the exact quenching mechanism, we examine  
275 a number of possible processes: enhanced radial diffusion with ions quenching rapidly on  
276 the edge of the main rings; the presence of an increased density of small charged grains  
277 on which the ions neutralize; enhanced H or H<sub>2</sub> emanating from Saturn's atmosphere or  
278 the ring atmosphere increasing the light ion density and quenching the heavy ions; an  
279 increased electron-ion recombination rate closer to the rings due to larger electron density  
280 and/or smaller electron temperatures.

### 281 ***Quenching by Diffusion***

282 The rate of plasma diffusion in the region of interest has not been examined in  
283 any detail. In *Tseng et al. (2013a)* we used a diffusion model consistent with data taken  
284 primarily outside the orbit of Enceladus (e.g., *Rymer et al., 2008; Sittler et al., 2008*).  
285 Extrapolating this model into our region, we used an average diffusion time of  $\sim 5 \times 10^6$ s.  
286 Such times are much too long to affect the radial dependence in the ion density extracted  
287 here. Further, due to the predicted radial dependence near the magnetic equator ( $\sim R^{-3}$ ),  
288 larger times occur at the smallest  $R$ , opposite to what would be required to explain our  
289 results. Finally, we also note that the ion temperatures vs.  $R$  in Fig. 5, particularly for  
290 2007, 2010, and 2012 data, are inconsistent with rapid inward diffusion.

291 Of course, the standard diffusion model might not be applicable in the region of  
292 interest. That is, there are significant and day/night asymmetries observed in the inner  
293 magnetosphere that are suggestive of an unexplained noon to midnight electric field  
294 (*Homberg et al., 2013*) or may related to the orbital varying Enceladus source. Although

295 the observations in the region of interest are sparse, variations in the ion speeds are  
296 comparable to the co-rotation speed and could enhance the effective diffusion rate. For  
297 instance, *Farrell et al. (2008)* interpreted their ‘down-drifting z-mode tones’ over the A-  
298 ring, measured by the Cassini RPWS instrument at SOI, as being due to rapid unloading  
299 of the plasma onto particles in the A-ring. They presumed the plasma diffused inward  
300 from the Enceladus torus source and quenched near the edge of the main rings at a rate of  
301  $\sim 40$  kg/s. This would be a significant fraction of the total ion production in the torus  
302 inside the orbit of Enceladus. This, in turn, would require diffusion times much more  
303 rapid than those discussed above in order to compete with the electron-ion  
304 recombination. Since these measurements were *only* available at SOI when the ring  
305 atmosphere was maximum and the magnetosphere was active, their observations are  
306 probably not applicable to others years. Rather, they are more likely consistent with the  
307 quenching of the relatively dense plasma formed just outside of the main rings from the  
308 extended ring atmosphere, which dominates the Enceladus torus source in the region of  
309 interest at SOI (*Elrod et al., 2012*).

### 310 ***Quenching on Small Grains***

311 Using the dust density observed by the CDA instrument, the ion-dust interaction  
312 did not significantly affect the ion loss or cooling in this region (*Tseng et al., 2013a*).  
313 However, there is likely a significant population of submicron-sized dust under the  
314 detection limit of this instrument ( $> 0.9\mu\text{m}$ ). As seen in Fig.1 the region inside  $3R_S$ ,  
315 contains the G-ring, the F-ring and the edge of the main rings in which collisions of small  
316 icy bodies produce debris (*Tiscareno et al., 2013; Attree et al., 2013*). This debris can  
317 deplete the energetic ions and electrons (*Paranicas et al., 2008; Cuzzi and Burns, 1988*)

318 as also seen in the CAPS background radiation (*Elrod, 2012*). Such debris, in the form of  
319 small grains, would be a sink for the thermal plasma with the required radial dependence  
320 (highest density at  $2.4R_S$  and lowest at  $3.8R_S$ ) suggestive of a ring source of small grains  
321 rather than an Enceladus source. Modeling indicates that the resulting dust/grain  
322 population typically follows a steep size distribution varying as  $1/r_g^a$  with  $a \sim 4-5$  where  
323  $r_g$  is the grain radius (*Kempf et al., 2008*). The ion-dust cross section can be written as  $[\pi$   
324  $r_g^2 (1 - U_g/E)]$  where  $U_g$  is the grain potential, which negative in this region (*Jurac et al.,*  
325 1996). Here  $E$  is either the thermal energy or the relative flow energy between the ion and  
326 the grain, depending on whether the grain has been accelerated to corotation or is in a  
327 Keplerian orbit with a speed relative to the corotating plasma of  $\sim 1.5 \times 10^6 \text{ cm s}^{-1}$  at  $2.5R_S$ .  
328 Presuming impacting ions neutralize on these grains, using an intermediate size  
329 dependence,  $\sim 1/r_d^{4.5}$ , and the relative speed above, with a density of  $1 \mu\text{m}$  grains of  $\sim$   
330  $2 \times 10^{-9}/\text{cm}^3$ , the density at  $2.5R_S$  would require a contribution from grains with radii down  
331 to  $\sim 10\text{nm}$ . However, the resulting density of small grains is large enough to significantly  
332 deplete the electrons, so that charged grains would dominate the total negative charge in  
333 this region. Evidence for this has not been seen, although if the small grain source was  
334 highly variable, it might contribute to the significant variability in the electron density in  
335 this region reported in *Persoon et al. (2013a)*.

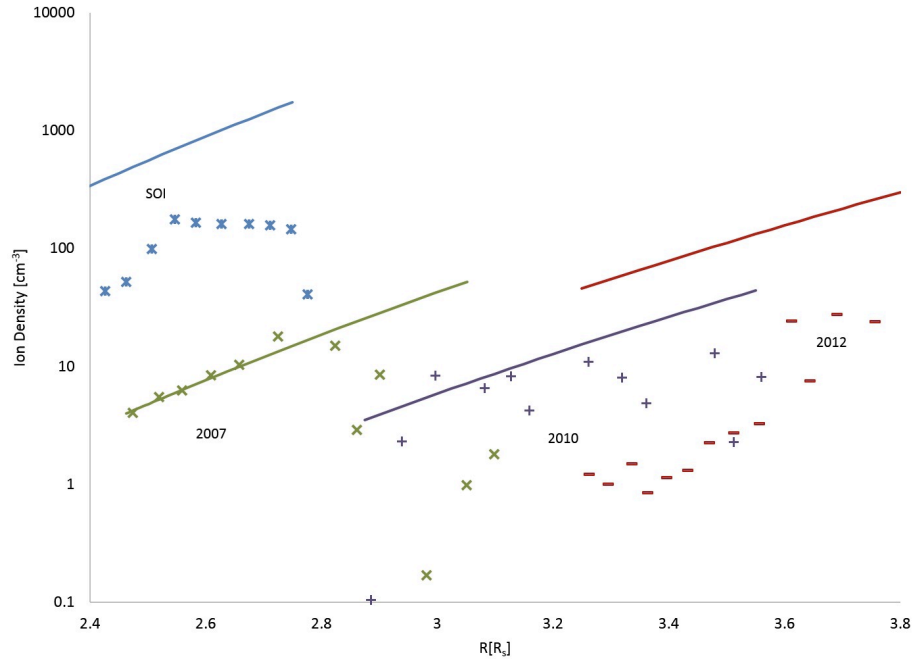
### 336 ***Quenching by Hydrogen from the Main Rings or Saturn***

337 In addition to the possible presence of small grains from the main and tenuous  
338 rings, the region outside of the main rings has significant levels of neutrals that decrease  
339 in density with increasing  $R$ . These are atoms and molecules from the icy ring particles  
340 (e.g., O, O<sub>2</sub> and H, H<sub>2</sub>; *Johnson et al., 2006a; Tseng et al., 2013b*) or H from Saturn

341 (*Shemansky et al.*, 2009; *Melin et al.*, 2009; *Tseng et al.*, 2013b). The light neutrals can  
342 react with the heavy ions changing the ion composition. However, with the exception of  
343 the important reaction,  $\text{H} + \text{O}^+ \rightarrow \text{H}^+ + \text{O}$ , these reactions do not result in a change in the  
344 *total* heavy ion density. Therefore, we find that an increased H population, which is also  
345 less readily ionized, does not appear to have a major effect on the ion density and  
346 composition (*Tseng et al.*, 2103a).

347         The presence of additional neutrals can also act to cool the electrons, especially if  
348 they are molecular. In *Tseng et al.* (2013a) we calculate electron density and temperature,  
349  $T_e$ , self-consistently with the production of and cooling of the ions. That is, we allow the  
350 photoelectrons produced to interact and cool by collisions with the molecules, hot  
351 electrons, and ions. Since the molecular ion neutralization rate increases with increasing  
352 electron density and with decreasing  $T_e$ , as  $\sim T_e^{-1/2}$ , the presence of additional neutrals as  
353 both a source of additional plasma and cooling of the electrons would cause the  
354 recombination rate to increase with decreasing  $R$ . If the enhanced cooling is due to  
355 molecules from the main rings produced by solar UV decomposition of ice particles, it  
356 would also be seasonal. That is, it would not be consistent with the dependence seen in  
357 Fig. 2: i.e., rapid quenching with decreasing  $R$  in 2007 when the seasonal ring atmosphere  
358 is predicted to be small. It would require a separate source from the edge of the rings,  
359 such as the inward diffusing high-energy background radiation.





360

361 Figure 6. Average ion density vs.  $R$ . Symbols (x,\*, +,-) are the rough estimates of the total light ion ( $H^+$ ,  
 362  $H_2^+$ ,  $H_3^+$ ) density, as discussed in the text: colors as in Fig. 2. For comparison, lines are the fits to the heavy  
 363 ion densities from Fig. 2.

364

365 ***Enhanced Light Ion Density***

366

As discussed above, the light neutrals can result in the production of light ions,

367

$H^+$ ,  $H_2^+$  and  $H_3^+$ . These are not included in the total heavy ion densities so that the radial

368

dependence of the total ion density might differ significantly from that for the heavy ions.

369

In Fig. 6 we use the CAPS data to extract *very rough* estimates of the light ion densities

370

and overlay them onto the fits for heavy ion densities in Fig. 2. Because the light ion

371

signal usually does not rise above the large background radiation in this region (*Elrod*

372

2012), these are rough estimates in which a ‘feature’ in the CAPS data is used when it is

373

seen, but are primarily estimated from the size of the background in the expected location

374

of the peak. Therefore, these results are only for guiding the discussion below.

375

In spite of the significant scatter, it is seen that the light ions apparently *can*

376

contribute significantly at the smaller values of  $R$  in Fig. 5. This is consistent with what

377 we find using the model in *Tseng et al.* (2013a). In our chemical model, H<sub>2</sub> from the ring  
378 atmosphere plays a significant role at SOI, primarily producing, H<sup>+</sup> and H<sub>2</sub><sup>+</sup>, that account  
379 for >50% of the total plasma from 2.5-3.0R<sub>S</sub>, larger than our rough estimates at SOI in  
380 Fig. 6. The light ion fraction decreases at larger R, roughly consistent with the trend in  
381 Fig. 6. Including the light ion contribution produced by H<sub>2</sub> from the ring atmosphere, our  
382 modeled rates still can not account for the heavy ion radial dependence measured at SOI.

383         Because of the uncertainties in the CAPS light ion densities, accurate  
384 measurements of the density and temperatures of the electrons in this region are critical.  
385 *Persoon et al.* (2013a,b) recently summarized the RPWS electron data, which they show  
386 is highly variable. Averaging over a number of Cassini orbits, their fit to that data inside  
387 the orbit of Enceladus suggests a much more slowly varying radial dependence ( $\sim R^4$ ;  
388 *Persoon et al.* 2013b) than that seen in Fig. 2 in the heavy ion data. However, as shown in  
389 *Elrod et al.* (2012) their densities at SOI are not inconsistent with our ion densities, and  
390 there is also rough agreement between their electron densities and the heavy ion densities  
391 in Fig. 2 at  $\sim 3.5R_S$ . This still allows that the electron densities at  $\sim 2.5R_S$  could be  
392 significantly greater than our measured heavy ion density for passes other than SOI. This  
393 would affect the recombination rates and suggest the presence of a significant component  
394 of light ions.

395         The 2007 data is interesting in that Cassini came reasonably close to the main  
396 rings at a time well past solstice when the contribution of O<sub>2</sub><sup>+</sup> from the ring atmosphere  
397 has been predicted to drop significantly (*Tseng et al.*, 2010). It is seen in Fig. 2 that there  
398 is significant scatter in the heavy ion data close to the ring, as the densities on the  
399 incoming and outgoing passes differ. It is also seen that the light ion densities in 2007 can

400 contribute significantly to the total ion density at the smallest values of  $R$ . RPWS electron  
401 data in 2007 soon to be published (*A. Persoon*, personal communication) suggest that  
402 inside  $\sim 2.9R_s$ , there is an upturn in the electron density near those values of  $R$  closest to  
403 Saturn where our light ion estimates appear to contribute significantly. As discussed  
404 above, such an upturn would be consistent with a source of light ions produced by  
405 coming from inside the region examined.

## 406 **5. Summary**

407 Including new data from post-equinox orbits, selecting only ion energy spectra  
408 which had significant counts above background, and averaging over passes occurring in  
409 the same year, we confirm that the near equatorial heavy ion density exhibits a significant  
410 temporal variation between 2004 and 2012 with a minimum near 2010. Although the  
411 ionization rate and photo-induced decomposition rate change during the solar cycle, the  
412 large variation in density and composition from SOI to equinox a seasonal effect appears  
413 to dominate. That is, the densities are very high and dominated by  $O_2^+$  nearest to southern  
414 solstice, are smallest close to equinox, and begin to increase post equinox, as seen from  
415 the fit parameter to the total ion density in Fig. 4. Although there will be no new data  
416 from the CAPS instrument to follow the growth to northern solstice, this interpretation  
417 appears to be supported by MIMI observations of energetic heavy ions (*Christon et al.*,  
418 2013) and most recently by the electron data (*Persoon et al.* 2013a). However, with the  
419 limited number of orbits in this region that have good data, we allow that other  
420 interpretations are possible and the relative importance of the ring atmosphere and solar  
421 activity needs to be explored further.

422 Surprisingly we also show that the heavy ion density exhibits a steep radial  
423 dependence over this narrow region (2.4 to 3.8 $R_S$ ), which appears to be roughly  
424 independent of the year. Our ion-neutral chemical model (*Tseng et al.*, 2013a) was able to  
425 describe the observed temporal dependence in the *average* density, composition and  
426 temperatures in this region. In this we used a seasonal ring atmosphere source (*Tseng et*  
427 *al.*, 2010) and Enceladus torus source (*Cassidy and Johnson*, 2010). This model also  
428 accounted for the surprisingly low ion temperatures found after SOI, seen again in the  
429 recently analyzed 2012 data set (Fig. 5). However, this model could not describe the  
430 observed radial dependence of the heavy ion density in Fig. 2, even allowing for the  
431 considerable uncertainties.

432 In the absence of the SOI data set, which is dominated by  $O_2^+$  supplied primarily  
433 by the ring atmosphere, one might conclude that the *average* densities in the other years  
434 are consistent with an Enceladus neutral torus source that is variable within the range  
435 suggested by *Smith et al.* (2010). In this case SOI would be exceptional, due to a robust  
436 ring atmosphere, with the contribution of the extended ring atmosphere negligible in  
437 2007-2012. If that is the case, then the radial dependence in the heavy ion density seen in  
438 those years might suggest that the models of the Enceladus neutral torus should decay  
439 more steeply than predicted with decreasing  $R$ . Since the distribution of neutrals in the  
440 torus depends nonlinearly on the density due to neutral-neutral collisions (*Cassidy and*  
441 *Johnson*, 2010; *Cassidy et al.*, 2011), if the densities are lower than those used the radial  
442 dependence would be steeper, as seen in models that neglect the neutral-neutral collisions  
443 (*Johnson et al.*, 2006; *Smith et al.*, 2010). Recently the variability seen by *Smith et al.*  
444 (2010) has been shown to be associated with the position of Enceladus in its orbit

445 (*Hedman et al.* 2013), so that the model of the neutral torus used in our ion chemistry  
446 model needs updating. Such work is now in progress and includes more detail,  
447 accounting for interactions with ice grains, the small moons, and the F & G rings within  
448 this region.

449         It is clear, however, that in spite of the large differences in the magnitude of the  
450 ion densities in going from 2004 to 2012, there is a similar radial trend over the narrow  
451 region (2.4 to 3.8  $R_S$ ). We point out that this cannot be due to rapid inward diffusion of  
452 ions formed from neutrals in the Enceladus torus, which *Farrell et al.* (2008) proposed to  
453 explain their SOI data. In the absence of good measurements of the light ion and electron  
454 densities for all passes, we suggest this dependence is primarily due to enhanced  
455 quenching of the heavy ion plasma with decreasing distance from the edge of the A-ring.  
456 Unless the ion diffusion rate in this region differs significantly from estimates at larger  $R$ ,  
457 the observed dependence is likely due to material emanating from smaller radial  
458 distances. Of particular interest is  $H_2$ , which plays an important role in our chemical  
459 model (*Tseng et al.* 2013a). A likely source is the significant, high-energy, background  
460 radiation, which diffuses inward and quenches on the particles in the tenuous rings and at  
461 the edge of the A-ring leading to production of  $H_2$  from the ice particles.

462         Since there will be no new CAPS data, understanding this neglected, but  
463 extremely interesting, region of the Saturnian system will require more detailed modeling  
464 of the extended ring atmosphere, the fate of the ring plasma, the role of the tenuous rings,  
465 the quenching of the high energy background radiation, and the variability in the  
466 Enceladus source in this region.

467

468 **6. Acknowledgements**

469 We acknowledge support through Southwest Research Institute from a grant for the  
470 Cassini Mission from JPL and by a grant from NASA's Planetary Atmospheres program.  
471 This work was also supported in part by National Aeronautics and Space Administration,  
472 Langley Research Center, under research cooperative agreement No. NNL09AA00A  
473 awarded to the National Institute of Aerospace.

474

475 **7. References**

476 Attree, N.O., C. D. Murray, G. A. Williams, N. J. Cooper, 2013. A Survey of Low-  
477 Velocity Collisional Features in Saturn's F Ring. *Astroph-EP*. arXiv 1309.3119v1  
478 Cassidy, T.A., R.E. Johnson, and A.R. Hendrix, 2011. Collisional Evolution of the  
479 Enceladus Neutral Cloud, 27th International Symp. on Rarefied Gas Dynamics, AIP  
480 Conf. Proc. 1333, 1133-1138 doi: 10.1063/1.3562796.  
481 Cassidy, T.A. and R.E. Johnson, 2010. Collisional spreading of Enceladus' neutral  
482 cloud, *Icarus* 209, 696-703.  
483 Christon, S.P., D. C. Hamilton, R. D. DiFabio, D. G. Mitchel, S. M. Krimigis, D. S.  
484 Jontof-Hutter, Saturn suprathermal  $O_2^+$  and mass-28<sup>+</sup> molecular ions: Long-term seasonal  
485 and solar variation, 2013. *J.Geophys. Res.* 28 JUN 2013 DOI: 10.1002/jgra.50383.  
486 Cuzzi, J.N., and J. A. Burns 1988. Charged particle depletion surrounding Saturn's  
487 F ring: Evidence for a moonlet belt? *Icarus* 74, 284–324  
488 Elrod, M.K., W.-L. Tseng, R.J. Wilson, R.E. Johnson, Seasonal Variations in Saturn's  
489 Plasma between the Main Rings and Enceladus, 2012. *J.Geophys.Res.* 117, A03207,  
490 doi:10.1029/2011JA017332.

491 Elrod, M.K. 2012. Seasonal Variations in Saturn's Plasma between the Main Rings  
492 and Enceladus PhD Thesis. The University of Virginia, Charlottesville, VA 22904

493 Farrell, W. M., M. L. Kaiser, D. A. Gurnett, W. S. Kurth, A. M. Persoon, J. E. Wahlund,  
494 and P. Canu, 2008. Mass unloading along the inner edge of the Enceladus plasma torus,  
495 *Geophys. Res. Lett.*, 35, L02203, doi:10.1029/2007GL032306

496 Holmberg, M.K.G., J.-E. Wahlund and M.W. Morooka, 2013. Day/night side asymmetry  
497 of ion densities and velocities in Saturn's inner magnetosphere EPSC Abstracts Vol. 8,  
498 EPSC2013-519, 2013 European Planetary Science Congress 2013.

499 Hedman, M.M., C. M. Gosmeyer, P. D. Nicholson, C. Sotin, R. H. Brown, R. N. Clark,  
500 K. H. Baines, B. J. Buratti, M. R. Showalter, 2013. An observed correlation between  
501 plume activity and tidal stresses on Enceladus. *Nature* **500**, 182–184.

502 Johnson, R.E., J.G. Luhmann, R.L. Tokar, M. Bouhram, J.J. Berthelier, E.C. Siler, J.F.  
503 Cooper, T.W. Hill, H.T. Smith, M. Michael, M. Liu, F.J. Crary, D.T. Young, Production,  
504 Ionization and Redistribution of O<sub>2</sub> Saturn's Ring Atmosphere, 2013a. *Icarus* 180, 393-  
505 402.

506 Johnson, R.E., Smith, H.T., Tucker, O.J., Liu, M., Burger, M.H., Sittler, E.C., Tokar,  
507 R.L., 2006b. The Enceladus and OH Tori at Saturn. *Astrophys. J.* 644, L137–L139.

508 Jurac, S., R.E. Johnson, R.A. Baragiola and E.C. Sittler, 1995. Charging of ice grains by  
509 low-energy plasma: Application to Saturn's E ring, *J. Geophys. Res.* 100,  
510 14,821-14,831.

511 Kempf, S., U. Beckmann, R. Srama, M. Horanyi, S. Auer, E. Grün, 2006 The  
512 electrostatic potential of E ring particles. *Planet. Space Sci.* 54, 999–1006.

513 Kempf, S.; Beckmann, U.; Moragas-Klostermeyer, G.; Postberg, F.; Srama, R.;

514 Economou, T.; Schmidt, J.; Spahn, F.; Grün, E. 2008. The E ring in the vicinity of

515 Enceladus. I. Spatial distribution and properties of the ring particles. *Icarus* 193, 420-437.

516 Martens, H.R., D.B. Reisenfeld, J.D. Williams, R.E. Johnson, and H.T. Smith, 2008.

517 Observations of molecular oxygen ions in Saturn's inner magnetosphere,

518 *Geophys.Res.Letts.* 35, L20103, doi:10.1029/2008GL035433.

519 Melin et al., 2009. The distribution of atomic hydrogen and oxygen in the magnetosphere

520 of Saturn, *Planetary and Space Science*, 57, 1743-1753.

521 Paranicas, C. , D.G. Mitchell, S.M. Krimigis, D.C. Hamilton, E. Roussos, N. Krupp, G.H.

522 Jones, R.E. Johnson, J.F. Cooper, T.P. Armstrong, 2008. Sources and losses of energetic

523 protons in Saturn's magnetosphere, *Icarus* 197, 519-525.

524 Persoon, A.M., D. A. Gurnett, J.-E. Wahlund, M. W. Morooka, W. S. Kurth, G. B.

525 Hospodarsky, and J. B. Groene. 2013a. Local Time Asymmetry and Seasonal Variations

526 of the Electron Density Distribution in Saturn's Inner Magnetosphere. Poster 2013 AGU

527 Meeting, San Francisco.

528 Persoon, A.M., D.A. Gurnett, J.S. Leisner, W.S. Kurth, J.B. Groene, and J.B. Faden,

529 2013b. The plasma density distribution in the inner region of Saturn's magnetosphere. *J.*

530 *Geophys. Res.* In press

531 Rymer et al Rymer, A. M.; Mauk, B. H.; Hill, T. W.; Paranicas, C.; Mitchell, D. G.;

532 Coates, A. J.; Young, D. T., 2008. Electron circulation in Saturn's magnetosphere. *J.*

533 *Geophys. Res.* 113, CiteID A01201. doi: [10.1029/2007JA012589](https://doi.org/10.1029/2007JA012589)

534 Shemansky, D. E.; X, Liu and H. Melin, 2009. The Saturn hydrogen plume, *Planet. Space*

535 *Sci.*, 57, 1659-1670.



536 Sittler, E. C., et al., 2008. Ion and neutral sources and sinks within Saturn's  
537 inner magnetosphere: Cassini results, *Planet. Space Sci.*, 56, 3–18.

538 Smith, H.T., R.E. Johnson, M.E. Perry, D.G. Mitchell, R.L. McNutt, D.T. Young, 2010.  
539 Enceladus plume variability and the neutral gas densities in Saturn's  
540 magnetosphere, *J.Geophys.Res.* 115, A10252, doi:10.1029/2009JA015184.

541 Tiscareno, M. S.; Mitchell, C, J.; Murray, C. D.; Di Nino, D.; Hedman, M. M.;  
542 Schmidt, J.; Burns, J. A.; Cuzzi, J. N.; Porco, C. C.; Beurle, K.; Evans, M.W, 2013.  
543 Observations of Ejecta Clouds Produced by Impacts onto Saturn's Rings. *Science* 340,  
544 460-464.

545 Tokar, R.L., R.E. Johnson et al., 2005. Cassini Observations of the Thermal Plasma in the  
546 Vicinity of Saturn's Main Rings and the F and G rings. *Geophys. Res. Letts.* 32, L14S04,  
547 doi:10.1029/2005GL022690.

548 Tseng, W.-L., R.E. Johnson, and M.K. Elrod, 2013a. Modeling the seasonal variability of  
549 the plasma environment in Saturn's magnetosphere between main rings and Mimas, *Plan*  
550 *& Space Sci.* 77, 126-135.

551 Tseng, W.-L., R.E. Johnson and W.-H. Ip, 2013b. The Atomic Hydrogen Cloud in the  
552 Saturnian System, *Planet. Space Sci.* in press.

553 Tseng, W.-L., . E. Johnson, M. F. Thomsen, T. A. Cassidy and M. K. Elrod, 2011.  
554 Neutral H<sub>2</sub> and H<sub>2</sub><sup>+</sup> ions in the Saturnian magnetosphere, *JGR* 116, A03209,  
555 doi:10.1029/2010JA016145.

556 Tseng, W.-L., W.-H. Ip, R.E. Johnson, T.A. Cassidy, and M.K. Elrod, 2010. The  
557 Structure and time variability of the ring atmosphere and ionosphere, *Icarus* 206, 382-  
558 389.